



Trends in temperature extremes over nine integrated agricultural regions in China, 1961–2011

Xushu Wu¹ · Zhaoli Wang¹ · Xiaowen Zhou¹ · Chengguang Lai^{2,3} · Xiaohong Chen^{2,3}

Received: 29 September 2015 / Accepted: 17 June 2016 / Published online: 30 June 2016
© Springer-Verlag Wien 2016

Abstract By characterizing the patterns of temperature extremes over nine integrated agricultural regions (IARs) in China from 1961 to 2011, this study performed trend analyses on 16 extreme temperature indices using a high-resolution ($0.5^\circ \times 0.5^\circ$) daily gridded dataset and the Mann-Kendall method. The results show that annually, at both daytime and nighttime, cold extremes significantly decreased but warm extremes significantly increased across all IARs. Overall, nighttimes tended to warm faster than daytimes. Diurnal temperature ranges (DTR) diminished, apart from the mid-northern Southwest China Region and the mid-Loess Plateau Region. Seasonally, DTR widely diminished across all IARs during the four seasons except for spring. Higher minimum daily minimum temperature (TNn) and maximum daily maximum temperature (TXx), in both summer and winter, were recorded for most IARs except for the Huang-Huai-

Hai Region; in autumn, all IARs generally encountered higher TNn and TXx. In all seasons, warming was observed at daytime and nighttime but, again, nighttimes warmed faster than daytimes. The results also indicate a more rapid warming trend in Northern and Western China than in Southern and Eastern China, with accelerated warming at high elevations. The increases in TNn and TXx might cause a reduction in agriculture yield in spring over Northern China, while such negative impact might occur in Southern China during summer. In autumn and winter, however, the negative impact possibly occurred in most of the IARs. Moreover, increased TXx in the Pearl River Delta and Yangtze River Delta is possibly related to rapid local urbanization. Climatically, the general increase in temperature extremes across Chinese IARs may be induced by strengthened Northern Hemisphere Subtropical High or weakened Northern Hemisphere Polar Vortex.

Electronic supplementary material The online version of this article (doi:10.1007/s00704-016-1848-0) contains supplementary material, which is available to authorized users.

✉ Zhaoli Wang
wangzhl@scut.edu.cn

¹ School of Civil Engineering and Transportation, South China University of Technology, Guangzhou 510641, China

² Center for Water Resources and Environment Research, Sun Yat-sen University, Guangzhou, China

³ Key Laboratory of Water Cycle and Water Security in Southern China of Guangdong High Education Institute, Sun Yat-sen University, Guangzhou, China

1 Introduction

Global climate change poses a potentially significant threat to worldwide food and drinking water supplies, as well as overall sustainable development (Easterling et al. 2000; IPCC 2014). Changes in the frequency of extreme temperatures are crucial to agricultural practices, energy demand, and human mortality (Wigley 1985; Frank 2005; Piao et al. 2010). It is commonly accepted that the global mean surface temperature has increased by about 0.74°C during the last century and is projected to increase another $1.8\text{--}4.0^\circ\text{C}$ in the coming century (Brohan et al. 2006; IPCC 2014). In the context of global warming, corresponding widespread and significant temperature extremes are expected to continue and as such are a

crucial consideration for governments, the public, and the climatic research community (Durre et al. 2000; Zhang et al. 2000; Luterbacher et al. 2004; Stott et al. 2004; Vincent and Mekis 2006; Miranda and Tome 2009; Otto et al. 2012; Almazroui et al. 2014; Sun et al. 2014; Viola et al. 2014).

China is a large (and largely agrarian) country with a total of nine integrated agricultural regions (IARs). A zoning system which divides the land mass of China into nine regions with similar temperatures, precipitation, and soil regimes has been adopted to simplify the analysis of climate changes according to different regions. Chinese sustainable agriculture development is related to the national grain safety, ecological safety, and development of the economy as a whole (Xu et al. 2002). Climate regimes and temperature changes in the IARs differ substantially from one to another. Studies on temperature extremes in the IARs are essential, because the impacts of extremes on national agriculture production are so significant. To date, numerous research projects have investigated these events at regional scale (Gao et al. 2014; Liang et al. 2014; Sun et al. 2014; Tao et al. 2014; Wang et al. 2014; Guan et al. 2015) and national scale (Zhai and Pan 2003; You et al. 2009; Zhang et al. 2011a; Wang and Fu 2013); however, relatively few studies have explored IARs and associated temperature extremes. As a consequence, there is lack of sufficient knowledge of the spatiotemporal variability of temperature extremes across IARs and no system of integrated information regarding temperature change extremes available for agriculture managers. To address this data shortage, this study quantitatively and synthetically examined the spatiotemporal variabilities of temperature extremes in all nine IARs in China.

Research on temperature extremes has traditionally been conducted based on station records (Zhai and Pan 2003; You et al. 2009; Wang and Fu 2013). Observational networks are imperfect, however, and possess many inherent problems such as inadequate station density and lack of long-term continuous observations (Abatzoglou 2013). Moreover, irregular distributions of the networks can reduce the spatial representativeness of the data on a large scale. Conversely, gridded data provides greater spatial representativeness and has been used in many more recent research projects (e.g., Donat and Alexander 2012). The present study utilized a high-resolution ($0.5^\circ \times 0.5^\circ$) daily gridded temperature dataset generated from 2474 meteorological stations across China. This dataset is the most recent gridded temperature dataset that has not yet been extensively used in any published studies on temperature extremes across China.

The primary goals of this study were, firstly, to synthetically research spatiotemporal changes in temperature extremes in each IAR, at both annual and seasonal scale;

secondly, to reveal the potential effects of these events on agriculture based on their observed changes; and, thirdly, to discuss the climatic and anthropogenic drivers of the extreme temperature variations across IARs. The remainder of this paper is arranged as follows: materials and methods are first described, followed by a discussion regarding the study results, then a brief summary and conclusion.

2 Data and methods

2.1 Data

The China Meteorological Administration (CMA) released a high-resolution ($0.5^\circ \times 0.5^\circ$) daily gridded temperature dataset in 2012. This gridded dataset was generated from 2474 Chinese meteorological stations through thin plate spline (TPS) and Global 30 Arc-Second Elevation (GTOPO30) data resampling. At each location, TPS interpolated the ratios of daily temperature to daily climatological values, eliminating the topographic effects on spatial interpolation. In this regard, TPS is particularly effective in regions with complex topography. This dataset is also the latest version of temperature dataset to cover the entirety of China (<http://cdc.cma.gov.cn/home.do>) and is only used in a few of recent literatures, e.g., Sun et al. (2015).

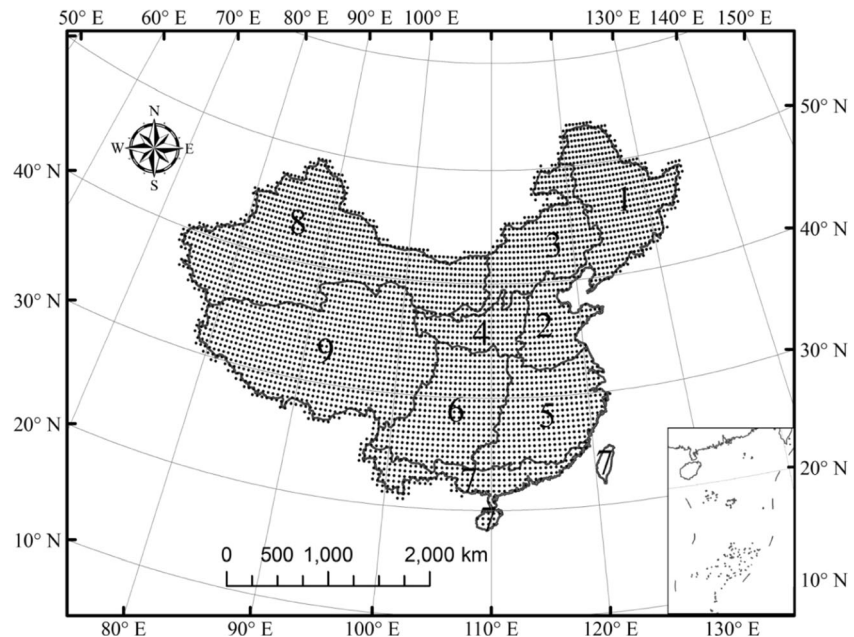
The National Meteorological Information Center (NMIC) performed a strict quality control procedure on the dataset and confirmed that annual mean biases of the mean, highest, and lowest temperatures between gridded and station datasets vary from -0.2 to 0.2 °C. The root-mean-square errors of the mean and lowest temperatures vary from 0.2 to 0.3 °C and from 0.2 to 0.5 °C, respectively, while that of the highest temperature is approximately 0.25 °C (Assessment Report of China's Ground Temperature $0.5^\circ \times 0.5^\circ$ Gridded Dataset V2.0, 2012). Therefore, the gridded dataset has altogether well sufficient accuracy to represent Chinese temperature characteristics. There are a total of 4189 grid points across China; the grid point locations, alongside the distributions of the nine IARs, are shown in Fig. 1.

For the purpose of investigating climate change impact on temperature extremes in China, the 74 atmospheric circulation indices were used and the data were obtained from the Climate Diagnostics and Prediction Division of the National Climate Center (<http://bcc.cma.gov.cn/en/>).

2.2 Extreme temperature indices

The Commission for Climatology (CCl)/Climate Variability and Predictability (CLIVAR)/Joint WMO-IOC

Fig. 1 The nine integrated agricultural regions and 4189 grid points in China. Numbers denote the agricultural regions: 1 Northeast China Region (IAR1); 2 Huang-Huai-Hai Region (IAR2); 3 Nei Mongol and along Great Wall Region (IAR3); 4 Loess Plateau Region (IAR4); 5 M and L Reaches of Changjiang River Region (IAR5); 6 Southwest China Region (IAR6); 7 South China Region (IAR7); 8 Gan-Xin Region (IAR8); and 9 Qinghai-Xizang Region (IAR9). Data in Taiwan are not available in the study



Technical Commission for Oceanography and Marine Meteorology (JCOMM) Expert Team on Climate Change Detection and Indices (ETCCDI) have recommended a suite of 16 temperature indices that cover many relevant aspects of temperature extremes (Zhang et al. 2011b, <http://ccma.seos.uvic.ca/ETCCDI>). These indices have been utilized often to research temperature extremes throughout the last several years and in many countries (Klein Tank et al. 2006; Li et al. 2012; Guan et al. 2015). As China has a complex climate regime (Wu et al. 2015), temperature features across different IARs may differ substantially from one another. Therefore, we employed all the 16 indices in order to comprehensively reflect temperature extremes in all of the IARs (Table 1).

2.3 Methodology

The Mann-Kendall (MK) method is commonly applied to trend analysis of time series (Mann 1945; Kendall 1975; Wu et al. 2015). The main advantage of MK is that the series being analyzed does not need to have any certain sample distribution, which prevents the potential interference of outliers. We chose the MK method because its robustness for non-normally distributed data and some of the climate indices may not follow a Gaussian distribution, as mentioned in previous research (Liang et al. 2014). This method is broadly used for examining trends of extreme temperature indices worldwide, e.g., Zhai and Pan (2003), Zhang et al. (2011a), and Viola et al. (2014). In the MK test, the null hypothesis, H_0 , indicates that data samples in the dataset are independent and

identically distributed with no trend. The prepared hypothesis, H_1 , states that there is a monotonic trend in the data samples. The algorithm can be described as follows.

Define a statistic S :

$$S = \sum_{i=1}^{n-1} \sum_{j=i+1}^n \text{sgn}(x_j - x_i) \quad (1)$$

in which

$$\text{sgn}(x_j - x_i) = \begin{cases} 1, & x_j - x_i > 0 \\ 0, & x_j - x_i = 0 \\ -1, & x_j - x_i < 0 \end{cases} \quad (2)$$

where S is a normal distribution with zero mean and variance $\text{var}(s) = n(n-1)(2n+5)/18$. Then, define another statistic, Z :

$$Z = \begin{cases} \frac{s-1}{\sqrt{\text{var}(s)}}, & s > 0 \\ 0, & s = 0 \\ \frac{s+1}{\sqrt{\text{var}(s)}}, & s < 0 \end{cases} \quad (3)$$

Given a level of confidence, α , if $|z| \geq z_{1-\alpha/2}$, then the null hypothesis must be rejected and the time series possesses a trend. Values of $z > 0$ indicate an upward trend and $z < 0$ a downward trend. The Kendall slope, which represents the magnitude of monotonic change, is as follows:

$$\beta = \text{Median} \left(\frac{x_j - x_i}{j-i} \right), \forall j < i \quad (4)$$

Table 1 Definitions of extreme temperature indices used in the study

Index	Descriptive name	Definition	Unit
CSDI	Cold spell duration indicator	Annual count of days with at least 6 consecutive days when $TN < 10$ th percentile	Days
DTR	Diurnal temperature range	Monthly mean difference between TX and TN	°C
FD	Frost days	Annual count when $TN < 0$ °C	Days
GSL	Growing season length	Annual (1 January–31 December in NH, 1 July–30 June in SH) count between first span of at least 6 days with daily temperature $TG > 5$ °C and first span after 1 July (1 January in SH) of 6 days with $TG < 5$ °C	Days
ID	Ice days	Annual count when $TX < 0$ °C	Days
SU25	Summer days	Annual count when $TX > 25$ °C	Days
TN10p	Cool nights	Percentage of days when $TN < 10$ th percentile	Days
TN90p	Warm nights	Percentage of days when $TN > 90$ th percentile	Days
TNn	Min T_{min}	Monthly minimum value of daily minimum temperature	°C
TNx	Max T_{min}	Monthly maximum value of daily minimum temperature	°C
TR20	Tropical nights	Annual count when $TN > 20$ °C	Days
TX10p	Cool days	Percentage of days when $TX < 10$ th percentile	Days
TX90p	Warm days	Percentage of days when $TX > 90$ th percentile	Days
TXn	Min T_{max}	Monthly minimum value of daily maximum temperature	°C
TXx	Max T_{max}	Monthly maximum value of daily maximum temperature	°C
WSDI	Warm spell duration indicator	Annual count of days with at least 6 consecutive days when $TX > 90$ th percentile	Days

NH, SH, TX, TN and TG denote the *NH* North Hemisphere, *SH* South Hemisphere, *TX* daily maximum temperature, *TN* daily minimum temperature, *TG* daily mean temperature

where $1 < i < j < n$. The estimator, β , is the median of all the combinations of record pairs for the entire data.

3 Results

3.1 Temporal trends

3.1.1 DTR trends

The annual trends of DTR in the nine IARs were demonstrated in Table 2. According to the trends and MK statistics, DTR showed a general downtrend in all of the IARs from 1961 to 2011. Moreover, except for the IAR4, 5, and 6, the remaining IARs all experienced significant declines in DTR. For China as a whole, DTR also decreased significantly.

3.1.2 Cold extremes (CSDI, FD, ID, TN10p, TNn, TX10p, and TXn)

As Table 2 shows, the cold extreme indices presented a consistent downtrend in all IARs, with the exception of TXn and TNn. There was a significant decrease in CSDI across all IARs except IAR6; specifically, all IARs experienced significant decreases in FD and TN10p. Significant downtrends in ID were found in all IARs except IAR6 and 7, while significant uptrends in TNn existed in all IARs except IAR4. There

was a general decrease in TX10p throughout the IARs, where only the trends in IAR2, 5, and 6 were insignificant over the entire measurement period. TXn exhibited a general uptrend in the IARs, with a particularly significant uptrend in both IAR5 and 6.

3.1.3 Warm extremes (GSL, SU25, TN90p, TNx, TR20, TX90p, TXx, and WSDI)

Note that GSL displayed a trend consistent with warming; the trends were all upward and statistically significant apart from in IAR7 (Table 2). It is also worth noting that prolonged GSL in the IARs is conducive to high agricultural yields. SU25 increased throughout all IARs, where only the trend in IAR2 was statistically insignificant. TN90p and TNx trends were upward and significant in all IARs. There was a general increasing trend in TR20 in all IARs at significance apart from IAR4. Similar to SU25, TX90p showed significant uptrends in all IARs with the exception of IAR2. TXx was observed to decrease in IAR2 but increased in the remaining IARs during the study period. All IARs experienced increasing WSDI, though the trends in IAR2 and 5 were not significant.

The above results reflect a considerable decline in cold extremes but an increase in warm extremes demonstrating a general warming environment throughout the IARs during 1961–2011. Additionally, decreased TN10p and TX10p together with

Table 2 Annual trends of the 16 temperature indices in the nine IARs and China

Index	IAR	1	2	3	4	5	6	7	8	9	China
CSDI	MK	-3.23	-3.01	-2.79	-3.27	-3.56	-1.84	-4.30	-3.92	-6.51	-5.66
	T	-0.76	-0.47	-0.70	-0.61	-1.02	-0.45	-1.79	-1.66	-1.75	-1.61
DTR	MK	-4.38	-5.53	-4.90	-0.43	-1.37	-0.59	-3.32	-6.73	-5.30	-6.21
	T	-0.21	-0.27	-0.20	-0.02	-0.05	-0.02	-0.09	-0.21	-0.17	-0.16
FD	MK	-5.53	-5.13	-6.08	-3.70	-4.10	-4.41	-4.55	-6.00	-6.10	-6.86
	T	-3.02	-4.64	-3.52	-2.44	-3.37	-2.43	-0.26	-3.54	-5.37	-3.61
GSL	MK	3.66	3.24	4.22	3.18	2.12	2.59	1.89	4.28	5.13	5.58
	T	2.61	3.78	3.31	3.25	2.31	1.90	0.06	2.58	5.17	3.08
ID	MK	-2.38	-1.97	-2.69	-3.29	-2.40	-1.78	-0.85	-2.26	-4.00	-4.20
	T	-1.75	-1.15	-2.16	-2.75	-0.19	-0.27	0.00	-1.61	-3.82	-1.73
SU25	MK	3.32	1.23	3.11	2.23	2.93	2.61	3.31	3.40	4.78	3.47
	T	2.85	1.11	2.87	1.95	2.62	1.92	3.11	1.60	0.43	1.80
TN10p	MK	-5.34	-5.71	-6.21	-5.26	-5.04	-4.04	-6.41	-6.73	-7.51	-7.43
	T	-2.37	-2.50	-2.49	-1.64	-1.60	-1.02	-2.02	-2.27	-3.17	-2.30
TN90p	MK	6.39	4.93	6.25	4.23	4.41	3.55	6.70	6.29	6.73	6.73
	T	2.04	2.17	2.25	1.67	1.62	1.22	2.97	2.55	3.05	2.34
TNn	MK	2.83	3.73	2.70	1.18	3.65	3.66	4.70	2.54	3.87	5.26
	T	0.70	0.64	0.50	0.18	0.44	0.31	0.48	0.42	0.51	0.48
TNx	MK	3.53	3.37	3.87	2.56	3.78	2.08	6.04	5.00	5.53	5.32
	T	0.32	0.21	0.40	0.20	0.19	0.08	0.20	0.37	0.31	0.28
TR20	MK	3.31	3.57	3.81	1.95	3.03	2.14	5.50	5.71	7.19	5.19
	T	0.93	3.08	0.66	0.54	2.19	1.01	4.32	1.77	0.21	1.32
TX10p	MK	-3.09	-1.78	-3.01	-3.14	-1.62	-0.59	-2.04	-3.06	-4.25	-4.04
	T	-1.04	-0.54	-0.97	-0.79	-0.33	-0.14	-0.41	-0.94	-1.35	-0.94
TX90p	MK	3.97	0.84	3.66	3.53	3.16	2.93	5.17	3.08	4.23	3.96
	T	1.23	0.32	1.34	1.49	1.26	1.15	1.82	1.13	1.72	1.26
TXn	MK	1.75	1.63	1.34	0.82	2.12	1.97	1.63	0.92	1.10	2.38
	T	0.48	0.25	0.26	0.16	0.33	0.22	0.19	0.19	0.14	0.27
TXx	MK	1.73	-0.40	1.24	1.80	1.63	1.70	2.10	2.33	3.48	2.98
	T	0.20	-0.06	0.18	0.19	0.12	0.11	0.11	0.16	0.26	0.17
WSDI	MK	3.98	0.93	3.70	2.55	1.78	2.12	3.92	2.28	2.95	3.32
	T	1.04	0.15	1.30	0.81	1.10	1.19	2.04	1.44	1.79	1.39

Values for the trends at the 0.05 significance level are shown in bold

IAR integrated agricultural region, MK MK statistics, T trends (per decade)

increased TN90p and TX90p reveal increasing air temperatures at both daytime and nighttime in all of the IARs.

3.2 Spatial distributions of trends

3.2.1 DTR trends

Significant DTR downtrends were observed throughout most of the IARs (Fig. 2). Specifically, DTR with growth rates smaller than $-0.2^{\circ}\text{C}/\text{decade}$ dominated almost all of IAR2 and most parts of IAR1, 3, and 8, as well as the middle of IAR9. Conversely, DTR generally increased in the mid-northern IAR6 and mid-IAR4.

3.2.2 Cold extremes (CSDI, FD, ID, TN10p, TNn, TX10p, and TXn)

Figure 3 portrays the spatial distributions of cold index trends in the IARs. There was a general decrease in CSDI in all IARs, with statistically significant downtrends in each except for IAR6. FD showed a significant downtrend throughout all IARs, and the effect was particularly pronounced in IAR9, where the growth rate was generally smaller than $-5\text{ days}/\text{decade}$. A reduction in ID was also detected for most of the IARs, where IAR3, 4, and 9 encountered a widely spread downtrend. The ID trend in IAR9 was especially notable, at a growth rate smaller than $-4\text{ days}/\text{decade}$. For TN10p, significant downtrends were widely distributed in all IARs

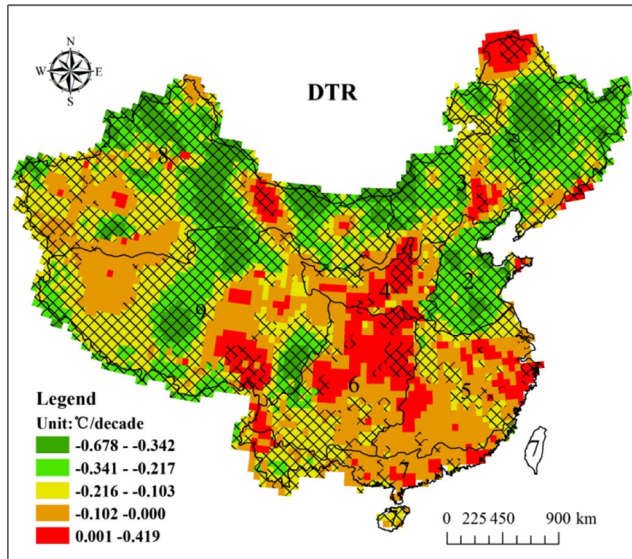


Fig. 2 Trends of annual DTR for 1961–2011. Hatching indicates regions where trends are significant at the 0.05 level

except for IAR6, where the northern parts showed the opposite. Decreasing TN10p was more apparent in IAR9 than in other IARs; the growth rates were generally smaller than -2 days/decade throughout IAR9. As opposed to TN10p, TNn showed a general uptrend in all IARs. Downtrends in TNn were observed, but they were rare and mostly not statistically significant. TX10p value also tended to decline, at mostly statistical significance, across all IARs. This trend was especially pronounced in IAR1, 3, 4, 8, and 9. IAR9 had decreasing TX10p with a growth rate generally smaller than -1 day/decade. For TXn, however, it presented a spatially heterogeneous pattern across all IARs.

3.2.3 Warm extremes (GSL, SU25, TN90p, TNx, TR20, TX90p, TXx, and WSDI)

The spatial pattern of the GSL trend appeared heterogeneous; IAR7 was characterized by insignificant downtrends in GSL, as opposed to IAR1, 2, 3, 4, and 8, which showed widespread significant uptrends (Fig. 4). For SU25, widespread and significant uptrends were found in all IARs except for IAR2 and 9. The northern parts of IAR1 and 3, as well as western IAR7, showed significant increases in SU25 with a growth rate larger than 3 days/decade. SU25 downtrends were prominent in almost the entirety of IAR9 and in mid-western IAR2. Overall warming trends were further confirmed as related to TN90p and TNx trends in the IARs. TN90p increased significantly across all IARs, with the only exception of a significant downturn in northern IAR6. In western IAR7, mid-IAR8, and southwestern IAR9, the growth rates of TN90p were larger than 2 days/decade. In most cases, TNx trends moved upward at statistical significance; specifically, the northern parts of IAR1 and 3, mid-IAR8, and western IAR9 showed increases

at growth rate larger than 0.3 °C/decade. TR20 displayed a heterogeneous distribution pattern across all IARs; IAR2 and 5 showed consistently increasing TR20 values that were mostly statistically significant, whereas IAR9 presented consistently insignificant downtrends. For the remaining IARs, TR20 trends showed spatial contrast. The spatial trend of TX90p was significantly upward across all IARs with the exception of IAR2, where TX90p exhibited a downward but insignificant trend. The TX90p growth rates in western parts of IAR7 and 9 were larger than 2 days/decade. TXx showed a heterogeneous distribution pattern that made the trends difficult to characterize accurately. As far as WSDI, a significant uptrend with a growth rate larger than 2 days/decades was found in the western parts of IAR7 and 9, whereas the remaining IARs showed decreasing WSDI at statistical significance in IAR1 and 3.

3.3 Seasonal variability of temperature extremes

In effort to establish a better and more comprehensive understanding of the extremes discussed above, the following section discusses an in-depth analysis of the seasonal changes related to temperature extremes. Because some of the temperature indices do not have seasonal changes (e.g., GSL), these indices were omitted from the original 16. Therefore, nine remaining indices were selected for further analysis: DTR, TN10p, TN90p, TNn, TNx, TX10p, TX90p, TXn, and TXx.

3.3.1 Temporal changes

Spring Insignificant uptrends in DTR were observed in IAR4, 5, and 6; the other IARs showed significant downtrends in the same season, however (Supplementary Table S1). TN10p generally decreased in value in all IARs, all at statistical significance except for IAR4 and 6. TN90p and TNn conversely increased, in fairly similar patterns, in all IARs from 1961 to 2011. More specifically, TN90p and TNn both significantly increased in IAR1, 2, 3, 8, and 9. In IAR7, the TN90p trend was upward but not significant, whereas TNn was statistically significantly upward. TNx had a consistent and significant uptrend in all IARs. TX10p increased throughout IAR6, 7, and 8 but decreased in the remaining IARs; IAR1 and 9 showed significant increases in TX10p, but the remaining IARs showed insignificant changes. TX90p, which is associated with warming trends, increased overall in all IARs during the measurement period; IAR4, 5, 6, and 7 were dominated by significant increases in TX90p. TXn presented a downturn in IAR6, 7, and 8 but an uptrend in the remaining IARs. IAR1 and 3 both experienced particularly significant increases in TXn. TXx increased consistently throughout all IARs, implying overall increases in maximum temperatures across China. Markedly significant TXx uptrends were observed in IAR4, 5,

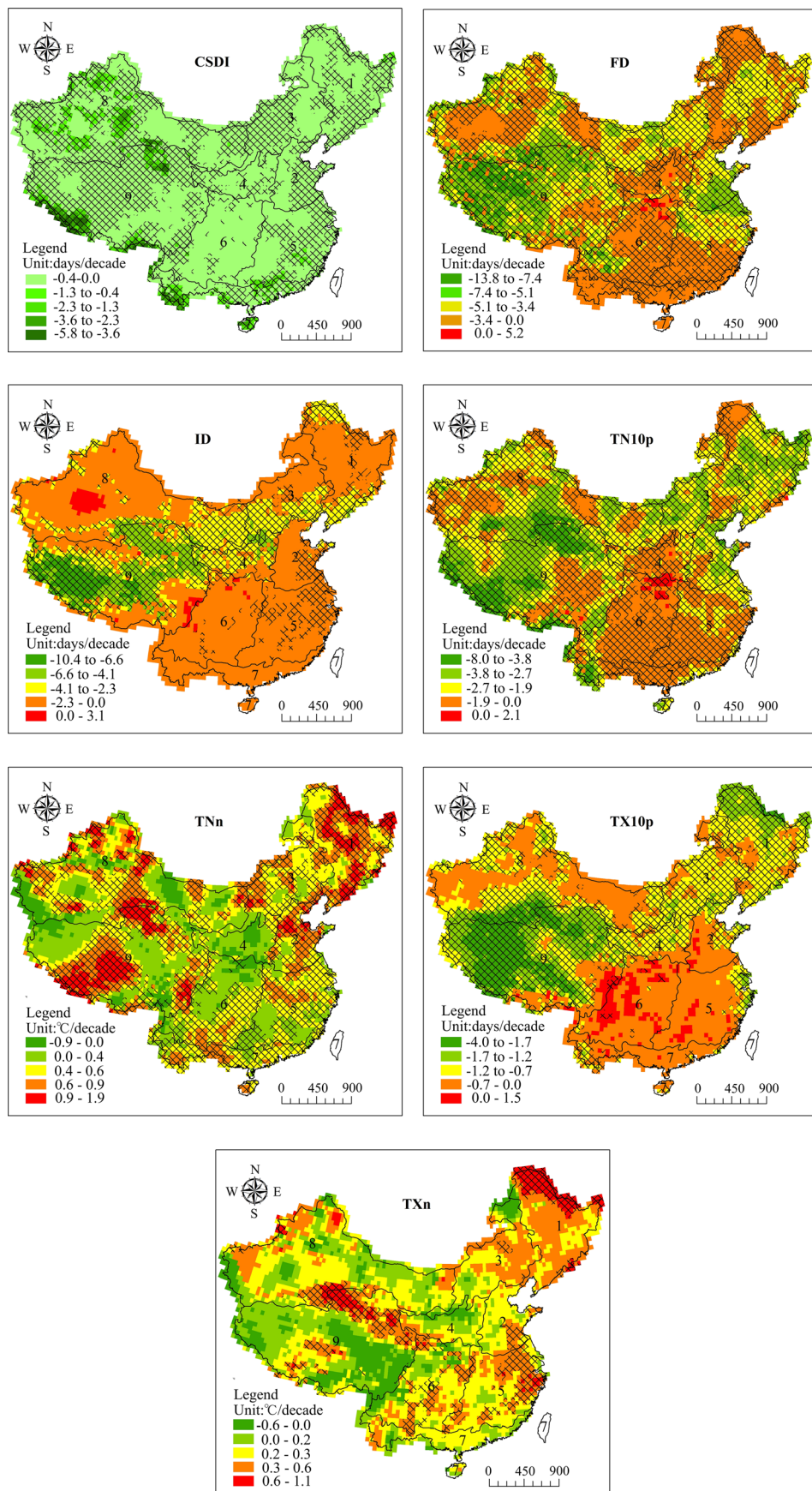


Fig. 3 Trends of annual cold extremes for 1961–2011. Hatching indicates regions where trends are significant at the 0.05 level

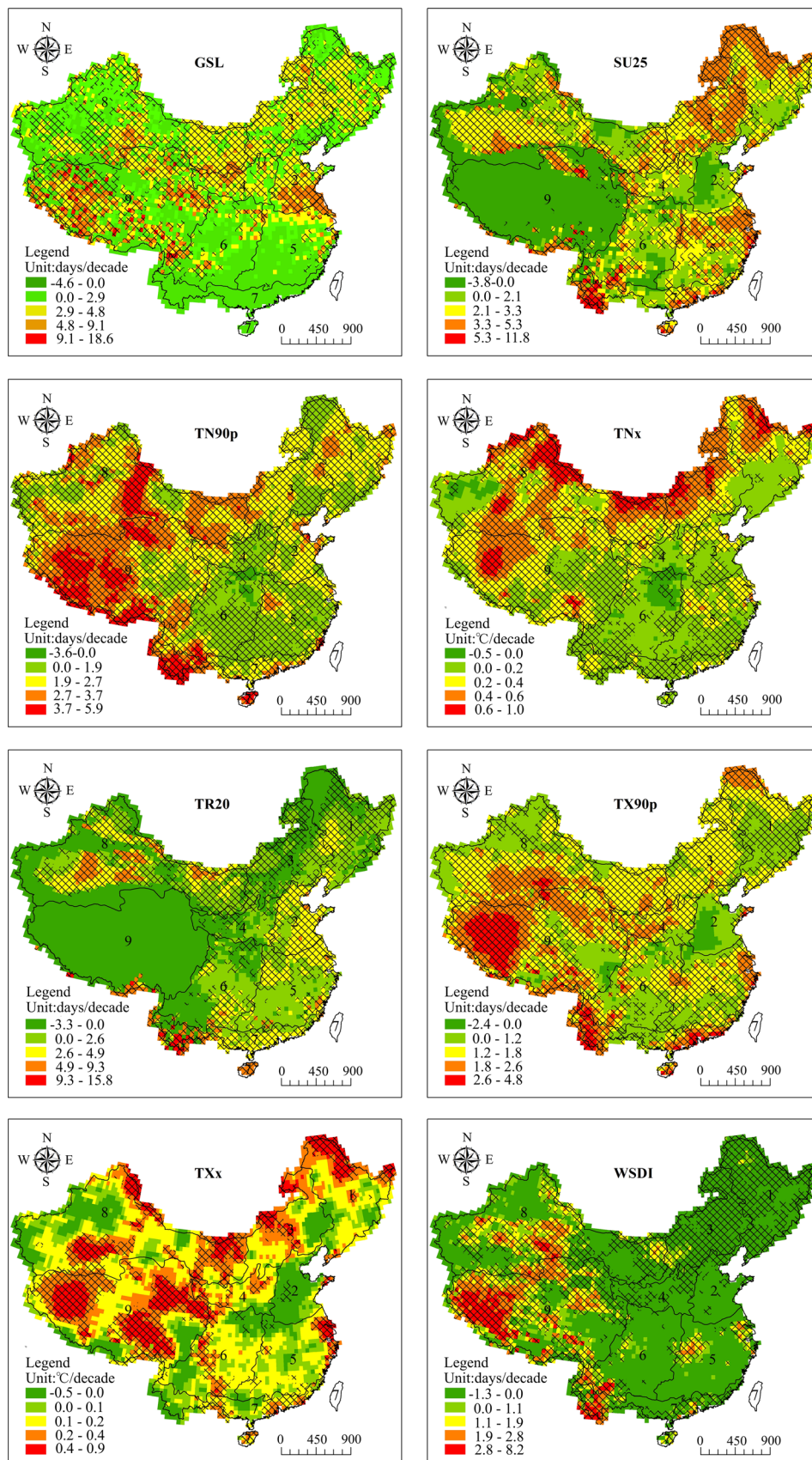


Fig. 4 Trends of annual warm extremes for 1961–2011. Hatching indicates regions where trends are significant at the 0.05 level

6, 7, and 8, though IAR1, 2, 3, and 9 showed insignificant increases.

Summer Decreasing trends in DTR characterized all IARs, at significance in IAR1, 2, 5, 8, and 9 (Supplementary Table S2). Significant downtrends in TN10p were pronounced in all IARs; conversely, uptrends of TN90p, TNn, and TNx dominated all IARs, at statistical significance with the only exception of TNn in IAR6. It is worth noting that TX10p decreased significantly in IAR1, 3, 7, 8, and 9, though it increased (insignificantly) in the remaining IARs. Although IAR2 showed a downward but not significant trend in TX90p, the remaining IARs were characterized by TX90p uptrends, at statistical significance except for IAR2 and 6. Significant uptrends were found in IAR1, 3, 7, 8, and 9 for TXn; downtrends were observed in the remaining IARs, though only that in IAR5 was statistically significant. Apart from IAR2, where TXx insignificantly decreased, all IARs showed increasing TXx. TXx trends in IAR5, 6, 7, 8, and 9 were significant, suggesting increased risk of extreme summer heat in these regions.

Autumn Slight increases in DTR occurred in IAR4 and 6 over the study period; statistically significant decreases in DTR were observed in IAR1, 2, 3, 8, and 9, however (Supplementary Table S3). TN10p exhibited a consistent and significant downtrend related to warming at nighttime across all IARs during the whole study period. There was a consistent and significant tendency toward increasing TN90p, TNn, TNx, and TX90p in the nine IARs. TX10p appeared to decrease in all of IARs but at significance only in IAR1, 4, 8, and 9. As for TNn, a significant uptrend spreads across all IARs. TXn also displayed a general uptrend in all IARs through the study period, at statistical significance in IAR7, 8, and 9. Moreover, significant increases in TXx were observed for all IARs except IAR1.

Winter The results demonstrate a consistent decreasing trend in DTR in all IARs (Supplementary Table S4). For IAR1, 2, 3, 7, and 8, DTR declined significantly in winters throughout the study period; basically, temperature ranges during winter generally shrank in China from 1961 to 2011. TN10p showed a more distinct downtrend over all of China compared to DTR; all IARs showed significant decreasing TN10p. TN90p, TNn, and TNx all increased from 1961 to 2011, with significant trends across all IARs. TX10p generally decreased in the IARs, though only the trends in IAR1, 4, and 9 were statistically significant. TX90p increased over time in all IARs, at statistical significance in IAR1, 3, 4, 7, 8, and 9. In terms of the changing pattern of TXn, we found likewise a general uptrend over China and, except for IAR7, 8, and 9, the remaining IARs had significant increasing TXn. In addition, TXx has decreased in IAR2 but it performed diversely in other

Table 3 Correlation coefficients between the 16 temperature indices, longitude, latitude, and elevation

Indices		Longitude	Latitude	Elevation
Diurnal temperature range	DTR	0.052	-0.356	0.067
Cold extremes	CSDI	0.223	0.147	-0.047
	FD	0.246	-0.106	-0.448
	ID	0.235	-0.119	-0.554
	TN10p	0.176	-0.129	-0.228
	TNn	0.179	0.185	-0.178
	TX10p	0.235	-0.240	-0.512
	TXn	0.353	0.292	-0.344
Warm extremes	GSL	-0.012	0.195	0.097
	SU25	0.435	0.210	-0.631
	TN90p	-0.358	-0.034	0.307
	TNX	-0.123	0.472	0.076
	TR20	0.087	-0.179	-0.460
	TX90p	-0.251	-0.118	0.285
	TXx	-0.035	0.159	0.197
	WSDI	-0.429	-0.208	0.401

Values that at the 0.05 significance level are shown in bold

IARs; the trends in IAR3, 4, 7, and 9 were statistically significantly upward.

Throughout China as a whole, all temperature indices for all seasons exhibited trends consistent with warming (Supplementary Table S1–4). In general, changes in the nine indices did not appear uniform across different seasons, even in the same IAR. That said, temperatures did clearly increase overall in all seasons, which is consistent with the annual results. Warming trends were present at both daytime and nighttime in all IARs, though nighttimes tended to warm faster than daytimes. All four seasons showed increasing minimum temperatures and maximum temperatures. There was particularly risk of extreme summer heat observed in IAR5, 6, 7, 8, and 9, owing to significant uptrends in summer TXx.

3.3.2 Spatial changes

Spring Significant decreasing trends in DTR were widely distributed throughout IAR1, 2, 3, 8, and 9, plus southwestern IAR6 and western IAR7. For most parts of IAR1, 2, and 3, the growth rates were smaller than $-0.2\text{ }^{\circ}\text{C}/\text{decade}$. On the contrary, uptrends were observed, mostly, in IAR4, 5, and 6 (Supplementary Fig. S1). There were general decreases in TN10p for all IARs. Except for IAR6 and 7, all IARs were characterized by a significant TN10p downtrends. IARs showed an altogether increasing TN90p, with significant uptrends in all IARs except IAR5 and 6. Areas with significant trends toward higher TNn were observed, spreading across nearly the entirety of IAR1, 2, and 3, as well as the middle of both IAR8 and 9 and northern IAR5. The growth rates in

IAR1 and 3 were particularly large, at over 0.5 °C/decade. Increasing TNx was also visible throughout all nine IARs, at statistical significance in each apart from IAR5 and 6. The growth rates in IAR1 were especially large, at above 0.4 °C/decade. TX10p decreased significantly in the northern part of IAR1, mid-IAR4, northeastern IAR5, and western IAR9, with growth rates smaller than -2 days/decade; however, significant increases in TX10p were observed in southwestern IAR6, with growth rates larger than 1 day/decade. Other regions mostly showed insignificant decreases in TX10p. A general increase in TX90p was visible across China, with significant uptrends distributed mainly throughout IAR4 and 5, northern IAR6, eastern and western IAR7, southern IAR8, and western IAR9. The fields showing significant trends in TX10p and TX90p also display less widespread spatial coverage than TN10p and TN90p, implying that warming trends at nighttime were more pronounced than at daytime. TXn values significantly increased in the majority of IAR1, northern IAR3, northeastern IAR5, and western IAR9 during the study period. The growth rates in IAR1 were mostly larger than 0.3 °C/decade. In other regions, however, TXn presented the same trends but below statistical significance. It should be noted that almost the entirety of IAR4, mid-IAR3, northern IAR5 and 6, eastern IAR8, and western IAR9 was subjected to higher TXx during the whole study period.

Summer DTR in the IARs decreased in most cases. For most parts of IAR1, 2, 5, 8, and 9, the trends were downward at statistical significance. Uptrends were also detected, but they were sporadically distributed in space (Supplementary Fig. S2). Similarly, TN10p showed a statistically significant uptrend in the majority of the IARs, and downtrends of TN10p were only found distributed in the northern IAR6. Regions apart from IAR6 showed significant increases in TN90p during 1961–2011. Western IAR9 was dominated by a significant increase in TN90p, with a growth rate larger than 14 days/decade. General increases in TNn, also, for all IARs, each at statistical significance except for IAR5 and 6. Consistent changes in TNx were also observed for all of IARs, while significant uptrends in TX10p, with growth rates larger than 1 day/decade, were observed in IAR5 and 6. Furthermore, TX10p declined significantly with a growth rate smaller than -5 days/decade in western and southern IAR9, however. For the remaining regions, TX10p showed largely insignificant downtrends. All parts of all regions apart from IAR2 and northern IAR6 showed increases in TX90p; however, statistically significant uptrends were irregularly distributed throughout space. IAR2 and northern IAR6 mostly encountered declines in TX90p, conversely. Regarding TXn changes, specifically, significant uptrends with growth rates larger than 0.3 °C/decade were dominant in most of IAR3 and mid-IAR8, whereas converse trends with growth rates smaller

than -0.1 °C/decade ran throughout IAR2, 4, 5, and 6. In general, TXx trends reflected summers growing hotter across the majority of the IARs from 1961 to 2011. The only exception is IAR2, which showed generally lower TXx during the study period.

Autumn The distribution pattern of DTR trends was spatially heterogeneous; except for IAR4, 5, 6, and 7, all IARs were characterized by a general decline in DTR. DTR did increase, notably, in IAR4 and 6 (Supplementary Fig. S3). TN10p also declined throughout almost all of China, at statistical significance in all IARs except for IAR5, 6, and 7. TN90p and TNn trends both behaved conversely to TN10p, showing widespread uptrends in all IARs. Significant uptrends in TNx were dominant across the IARs, with the exception of IAR5. Both uptrends and downtrends in TX10p were observed in all IARs, but the downtrends were more prominent. IAR9 experienced a particularly significant decline in TX10p, with a growth rate smaller than -4 days/decade. TX90p displayed a general uptrend, and, except for IAR2, the remaining IARs showed statistically significant increases. Although downtrends in TXn occurred in some parts of IAR2, 4, 5, 6, and 9, the seasonal occurrence of TXn presented overall uptrends across the IARs. Mid-IAR8 and northern and western IAR9 encountered significant increases in TXn with growth rates larger than 0.4 °C/decade. TXx also featured uptrends in all IARs, at statistical significance in IAR3, 4, and 8, as well as northern parts of IAR5 and 6 and northern and western IAR9. The growth rates in these regions also were generally larger than 0.3 °C/decade.

Winter IAR1, 2, 3, and 8 were characterized by decreasing, statistically significant DTR values (Supplementary Fig. S4). DTR uptrends were observed but only in IAR9. There was a widespread coherent and significant downtrend in TN10p over all nine IARs. TN10p, TN90p, TNn, and TNx all displayed general increasing trends in all IARs. TN10p and TNx uptrends were particularly significant in all IARs except for IAR5 and 6, whereas increasing TN90p was significant in every single IAR. The growth rates of TN90p in IAR1 were especially high, above 0.6 °C/decade. TX10p was marked by a general downtrend in the nine IARs. For the majority of IAR4, plus eastern and northern IAR1 and middle and northern IAR9, TX10p generally declined, with growth rates smaller than -3 days/decade. In addition, despite decreases in TX90p detected in small parts of IAR2, 5, and 6, all IARs exhibited overall increases in TX90p consistent with warming. In western IAR7 and 9, the growth rates of TX90p were larger than 8 days/decade. A generally significant uptrend in TXn was observed, mainly distributed in IAR1, 2, 3, and 4, where growth rates were larger than 0.3 °C/decade. Widespread increases in TXx were also observed in all IARs,

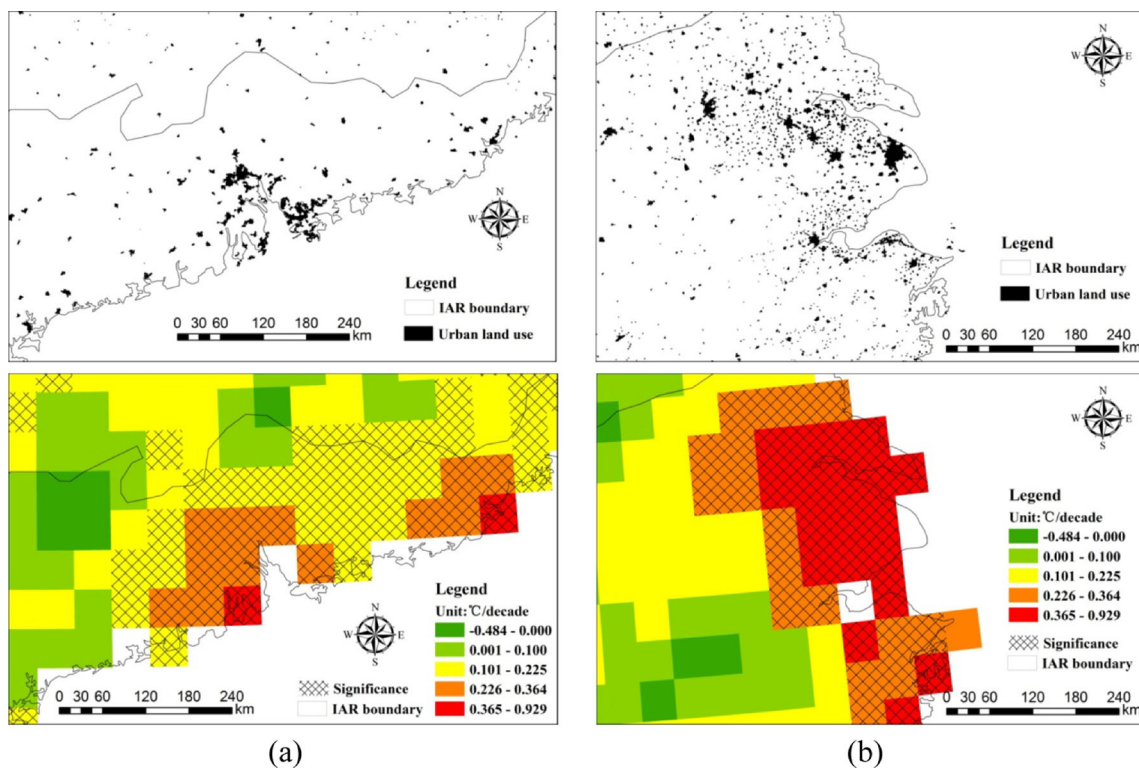


Fig. 5 TXx trends and urban land use in the **a** Pearl River Delta and **b** Yangtze River Delta. Figures of urban land use are presented above those of TXx trends

apart from IAR2, which did show a downtrend. The most significant TXx uptrends, with growth rates larger than 0.5 °C/decade, were predominantly distributed throughout

IAR9. Average maximum winter temperatures across the whole of China during the study period have increased overall, especially within IAR9.

Table 4 Correlation coefficients between the 16 temperature indices and ANHSHI

IAR	1	2	3	4	5	6	7	8	9	China
CSDI	-0.174	-0.335	-0.337	-0.454	-0.527	-0.496	-0.556	-0.450	-0.471	-0.568
DTR	-0.598	-0.330	-0.506	0.252	-0.046	0.094	-0.158	-0.531	-0.348	-0.472
FD	-0.551	-0.512	-0.577	-0.386	-0.501	-0.605	-0.590	-0.631	-0.624	-0.689
GSL	0.294	0.371	0.394	0.436	0.103	0.271	0.045	0.520	0.591	0.581
ID	-0.310	-0.317	-0.431	-0.570	-0.253	-0.357	-0.201	-0.438	-0.395	-0.604
SU25	0.276	0.348	0.349	0.414	0.481	0.500	0.676	0.366	0.560	0.532
TN10p	-0.477	-0.533	-0.565	-0.532	-0.532	-0.588	-0.714	-0.649	-0.622	-0.671
TN90p	0.675	0.628	0.661	0.566	0.726	0.645	0.764	0.669	0.621	0.713
TNn	0.284	0.338	0.302	0.144	0.359	0.385	0.633	0.321	0.346	0.513
TNx	0.273	0.415	0.336	0.300	0.727	0.511	0.827	0.350	0.596	0.529
TR20	0.255	0.395	0.338	0.288	0.453	0.496	0.715	0.478	0.614	0.575
TX10p	-0.234	-0.286	-0.278	-0.508	-0.322	-0.374	-0.583	-0.370	-0.483	-0.506
TX90p	0.471	0.339	0.537	0.546	0.488	0.535	0.737	0.505	0.531	0.621
TXn	0.194	0.149	0.127	0.171	0.265	0.361	0.434	0.185	0.156	0.318
TXx	0.153	-0.051	0.160	0.221	0.350	0.294	0.610	0.145	0.464	0.367
WSDI	0.469	0.290	0.484	0.438	0.426	0.416	0.588	0.437	0.483	0.567

Values that at the 0.05 significance level are shown in bold

Table 5 Correlation coefficients between the 16 temperature indices and SNHSHI

IAR	1	2	3	4	5	6	7	8	9	China
CSDI	-0.149	-0.310	-0.322	-0.427	-0.492	-0.462	-0.524	-0.420	-0.435	-0.527
DTR	-0.589	-0.328	-0.473	0.257	-0.035	0.107	-0.131	-0.498	-0.319	-0.443
FD	-0.534	-0.486	-0.561	-0.366	-0.482	-0.601	-0.563	-0.619	-0.652	-0.686
GSL	0.266	0.340	0.358	0.430	0.080	0.266	0.040	0.514	0.622	0.575
ID	-0.265	-0.300	-0.408	-0.561	-0.261	-0.378	-0.181	-0.444	-0.417	-0.602
SU25	0.260	0.330	0.365	0.428	0.488	0.521	0.700	0.389	0.573	0.545
TN10p	-0.437	-0.510	-0.521	-0.521	-0.517	-0.595	-0.698	-0.629	-0.615	-0.648
TN90p	0.664	0.624	0.658	0.572	0.742	0.685	0.793	0.678	0.645	0.727
TNn	0.232	0.307	0.258	0.107	0.333	0.367	0.596	0.294	0.352	0.470
TNx	0.248	0.429	0.335	0.307	0.737	0.513	0.831	0.362	0.598	0.531
TR20	0.248	0.393	0.343	0.305	0.473	0.529	0.732	0.495	0.609	0.591
TX10p	-0.189	-0.258	-0.241	-0.507	-0.319	-0.397	-0.615	-0.381	-0.512	-0.506
TX90p	0.457	0.338	0.550	0.563	0.508	0.560	0.774	0.522	0.556	0.641
TXn	0.137	0.108	0.071	0.131	0.248	0.371	0.432	0.165	0.195	0.286
TXx	0.154	-0.024	0.195	0.267	0.375	0.311	0.615	0.166	0.461	0.390
WSDI	0.485	0.314	0.506	0.459	0.454	0.441	0.647	0.449	0.498	0.592

Values that at the 0.05 significance level are shown in bold

To summarize, overall temperature ranges in Chinese IARs during summer and winter have mostly diminished since the 1960s, while temperature ranges in spring and autumn have not shown spatial coherence. In both summer and winter, increasing minimum and maximum temperatures throughout the study period were common across all IARs, with one exception where decreased maximum temperatures in IAR2

during summer and winter were observed. In autumn, minimum and maximum temperatures have generally increased; in spring, patterns of minimum and maximum temperatures were spatially heterogeneous. Warming trends were apparent for all seasons, in both daytime and nighttime, across all of China during the entire study period. Warming at nighttime was consistently more pronounced than at daytime.

Table 6 Correlation coefficients between the 16 temperature indices and ANHPVI

IAR	1	2	3	4	5	6	7	8	9	China
CSDI	0.367	0.562	0.447	0.388	0.422	0.333	0.523	0.421	0.507	0.604
DTR	0.354	0.572	0.394	0.069	0.162	0.069	0.279	0.530	0.440	0.505
FD	0.697	0.704	0.753	0.596	0.566	0.573	0.431	0.727	0.743	0.821
GSL	-0.550	-0.462	-0.618	-0.474	-0.364	-0.436	-0.006	-0.638	-0.686	-0.790
ID	0.469	0.385	0.530	0.392	0.307	0.193	0.163	0.434	0.426	0.655
SU25	-0.457	-0.232	-0.514	-0.379	-0.391	-0.429	-0.514	-0.513	-0.595	-0.594
TN10p	0.651	0.733	0.732	0.698	0.692	0.611	0.698	0.713	0.668	0.781
TN90p	-0.758	-0.732	-0.797	-0.682	-0.611	-0.596	-0.690	-0.733	-0.676	-0.762
TNn	-0.424	-0.401	-0.367	-0.019	-0.314	-0.308	-0.449	-0.274	-0.354	-0.524
TNx	-0.546	-0.489	-0.553	-0.423	-0.507	-0.337	-0.598	-0.598	-0.684	-0.712
TR20	-0.526	-0.546	-0.581	-0.373	-0.491	-0.429	-0.627	-0.672	-0.675	-0.705
TX10p	0.573	0.417	0.611	0.491	0.376	0.308	0.440	0.518	0.544	0.690
TX90p	-0.707	-0.220	-0.655	-0.452	-0.477	-0.472	-0.641	-0.565	-0.545	-0.662
TXn	-0.347	-0.242	-0.229	-0.132	-0.337	-0.259	-0.244	-0.212	-0.150	-0.384
TXx	-0.213	0.052	-0.253	-0.220	-0.281	-0.294	-0.479	-0.322	-0.408	-0.429
WSDI	-0.628	-0.207	-0.547	-0.323	-0.219	-0.278	-0.437	-0.478	-0.435	-0.534

Values that at the 0.05 significance level are shown in bold

Table 7 Correlation coefficients between the 16 temperature indices and SNHPVI

IAR	1	2	3	4	5	6	7	8	9	China
CSDI	0.181	0.358	0.265	0.368	0.455	0.301	0.435	0.350	0.465	0.486
DTR	0.499	0.454	0.358	-0.131	0.112	-0.003	0.169	0.496	0.478	0.489
FD	0.488	0.445	0.503	0.371	0.276	0.411	0.416	0.666	0.763	0.682
GSL	-0.164	-0.281	-0.303	-0.475	-0.082	-0.245	-0.078	-0.597	-0.721	-0.609
ID	0.088	0.109	0.192	0.284	0.083	0.102	0.150	0.218	0.492	0.423
SU25	-0.407	-0.124	-0.503	-0.359	-0.431	-0.485	-0.634	-0.431	-0.614	-0.577
TN10p	0.408	0.486	0.434	0.496	0.507	0.555	0.631	0.553	0.697	0.627
TN90p	-0.545	-0.544	-0.568	-0.543	-0.614	-0.615	-0.754	-0.674	-0.757	-0.715
TNn	-0.256	-0.280	-0.185	-0.056	-0.162	-0.274	-0.435	-0.121	-0.465	-0.387
TNx	-0.424	-0.434	-0.583	-0.467	-0.600	-0.454	-0.709	-0.537	-0.699	-0.690
TR20	-0.383	-0.431	-0.544	-0.467	-0.497	-0.555	-0.678	-0.623	-0.725	-0.682
TX10p	0.180	0.175	0.192	0.407	0.166	0.272	0.454	0.289	0.580	0.447
TX90p	-0.387	-0.159	-0.520	-0.484	-0.459	-0.529	-0.732	-0.491	-0.568	-0.600
TXn	-0.209	-0.080	-0.050	0.020	-0.150	-0.230	-0.331	-0.004	-0.264	-0.207
TXx	-0.228	0.037	-0.378	-0.369	-0.246	-0.293	-0.468	-0.320	-0.373	-0.455
WSDI	-0.447	-0.102	-0.487	-0.322	-0.354	-0.406	-0.686	-0.399	-0.504	-0.545

Values that at the 0.05 significance level are shown in bold

4 Discussion

4.1 Summary of the observed changes in temperature extremes

Analyses of extreme temperature trends, established using the 51-year length of gridded data (1961–2011) gathered across China, reveal widespread and significant changes related to warming. Annually, there were significant declines in cold extremes but significant increases in warm extremes observed in the IARs overall. Average temperatures increased at both daytime and nighttime, but nighttimes warmed faster than daytimes. These results are consistent with the results obtained in other global temperature studies (Alexander et al. 2006) as well as regional studies (Zhai and Pan 2003; Fan et al. 2011; Almazroui et al. 2014; Gao et al. 2014; Guan et al. 2015). Seasonally, temperatures again were observed to increase overall at both daytime and nighttime, and again, nighttimes warmed faster than daytimes. These results are in accordance with previous studies (Zhai and Pan 2003).

4.2 Potential effects of extreme temperature variability on agriculture

Previous studies have confirmed the influences of daily minimum and maximum temperatures on agriculture yield (Skaggs and Irmak 2012; Zhang et al. 2016). An increase in daily maximum temperature can enhance transpiration and plant water stress, resulting in greater water requirements for

agriculture production, while an increase in daily minimum temperature, which often occurs at nighttime, can accelerate plant respiration and increase dry matter consumption by the plants, causing reduction in agriculture yield. The recorded significant increased TNn in IAR1, 2, and 3, and TXx in IAR4 during spring might suggest a reduction in agriculture yield in these IARs in spring seasons (Supplementary Fig. S1). Significant increased TNn in all of IARs except for IAR5 and 6 in summer might also have negatively impacted plant productivity (Supplementary Fig. S2). In autumn and winter seasons, however, widespread increases in TNn and TXx were seen, which indicates possibly a general reduction in agriculture yield across China (Supplementary Fig. S3–4).

4.3 Relationships between longitude, latitude, elevation, and extreme temperature trends

The absolute values of growth rates of temperature extremes in IAR5, 6, and 7 were generally smaller than those in the remaining IARs (Table 2). The relationships between extreme temperature trends, longitude, latitude, and elevation were also analyzed (Table 3). As Table 3 shows, most of the cold indices declined faster at high latitudes than at low latitudes. In contrast, the cold indices generally declined faster at low longitudes than at high longitudes. By extension, Northern and Western China warmed faster than Southern and Eastern China; these phenomena were also observed by Yang et al. (2014). Cold extremes tended to decrease more rapidly at higher elevations, indicating accelerated warming at high

elevations in China. This finding is supported by other global research projects (Beniston and Rebetez 1996; Beniston 2003) and likely implies more rapid decreases in certain cold extreme indices (e.g., TX10p and ID) for the Qinghai-Tibet plateau (located in IAR9) than for other regions (Fig. 3). An earlier study by Tian et al. 2006 reported a larger warming trend in Eastern Pamirs than in other parts of China. Similarly, You et al. (2008) revealed a correlation between TX10p, TXn, and elevation in the eastern and central parts of the Tibet plateau. Warm extremes seemed to have weaker relationships with longitude, latitude, and elevation, however, as their correlations were relatively ambiguous (Table 3).

4.4 Possible climatic and anthropogenic drivers

The observed changes in temperature extremes over Chinese IARs can be attributed to several climatic and anthropogenic factors. Previously, Zhou and Ren (2011) asserted that large-scale circulations and urbanization are two of the main factors impacting Chinese temperature extremes. Ren et al. (2012) proposed at least a 27 % contribution from urbanization to warming trends in China from 1960 to 2004. Sun et al. (2014) reported increasing frequency of extreme summer heat in Eastern China, attributable to the anthropogenic emission of greenhouse gases associated with rapid urbanization.

This study built preliminary and qualitative analyses of the relationships between Chinese urbanization and the 16 temperature indices by visually comparing the significant index fields shown in Figs. 3 and 4 with the urbanized areas in China. Apart from TXx, all indices showed weak spatial coherence with urbanization. The urbanization fields in the Pearl River Delta (PRD) and Yangtze River Delta (YRD), specifically, matched well with the significant fields of annual TXx trends in these regions (Fig. 5). The growth rates of TXx in PRD and YRD were prominent and larger than those of the surrounding regions. Therefore, local rapid urbanizations in PRD and YRD possibly resulted in higher TXx during recent decades.

It is pointed out that global warming has increased concurrent climatic extremes such as extreme heat waves (AghaKouchak et al. 2014). Temperature extremes are possibly induced by circulation changes that are driven by different warming over land and the sea (Vallis et al. 2015). We argued that the observed extreme temperature variability may result from circulation changes related to global warming and subsequently examined the relationships between 74 circulation indices and the 16 temperature indices in each IAR. Variations in the Northern Hemisphere Subtropical High (NHS) and Northern Hemisphere Polar Vortex (NHPV), as the result suggested, were found to be two major factors that influenced temperature changes across China. Tables 4, 5, 6, and 7 show the correlation coefficients between the area of the NHS index (ANHSI), strength of the NHS index (SNHSI),

area of the NHPV index (ANHPVI), strength of the NHPV index (SNHPVI), and the 16 temperature indices in all IARs, respectively. There exist generally significant, positive relationships between ANHSI, SNHSI, and warm indices and generally significant, negative relationships between ANHSI, SNHSI, and cold indices (Tables 4 and 5). However, the correlations between ANHPVI, SNHPVI, and temperature indices are mostly opposite to those between ANHSI, SNHSI, and the temperature indices. Generally significant, negative relationships were detected between ANHPVI, SNHPVI, and warm indices, whereas generally significant, positive relationships were found between ANHPVI, SNHPVI, and cold indices (Tables 6 and 7). These results are in agreement with relevant researches (Gu and Yang 2006; Zhang et al. 2013; Liang et al. 2014). Strengthened NHS and/or weakened NHPV possibly induce increased temperature extremes in Chinese IARs; nevertheless, it is important to note that climatic changes impacting temperature extremes in China are a complex issue, and the mechanisms involved necessitate further study.

5 Conclusions

The present study analyzed temperature extremes in nine Chinese IARs using a high-resolution ($0.5^\circ \times 0.5^\circ$) gridded temperature dataset from 1961 to 2011. The MK method was applied for all analyses. The most notable findings of the study can be summarized as follows:

- Annually, at both daytime and nighttime, all IARs were characterized by significant declines in cold extremes but significant increases in warm extremes. The warming observed at nighttime was more pronounced than that at daytime. From 1961 to 2011, DTR diminished overall except for the mid-northern part of IAR6 and mid-IAR4. In addition, SU25 increased significantly in northern IAR1 and 3 and western IAR7, while significant increases in TR20 were observed in IAR2 and 5.
- DTR values in summer and winter seasons, specifically, widely diminished over the course of the study period. In spring and autumn, however, DTR diminished in IAR1, 2, 3, 8, and 9 but enlarged in IAR4 and 6. Increasing TNn and TXx values were recorded across all IARs except for IAR2 in summer and winter. In autumn, TNn and TXx generally increased, whereas the patterns of TNn and TXx in spring were spatially heterogeneous. Warming trends were clearly observed for both daytime and nighttime in all seasons, and warming at nighttime was more pronounced than at daytime.
- Northern and Western China seemed to warm faster than Southern and Eastern China, overall, and further accelerated warming was possible at high elevations.

- Spring temperature extremes might have negative impacts on agriculture yield in Northern China, whereas these events in summer might negatively impacted agriculture yield in Southern China. In autumn and winter, temperature extremes might cause a general reduction in agriculture yield over China.
- Temperature extremes in the IARs showed weak correlations with urbanization. One exception is where TXx in PRD and YRD was possibly related to local, rapid urbanization. Climatically, both NHSH and NHPV possibly influenced temperature extremes in the IARs; strengthened NHSH and/or weakened NHPV are able to induce increased temperature extremes across China.

Acknowledgments The research is financially supported by the National Natural Science Foundation of China (Grant No. 51209095, 51579105), the National Science and Technology Support Program (Grant No. 2012BAC21B0103), and the Fundamental Research Funds for the Central Universities (2014ZZ0027).

References

- Abatzoglou JT (2013) Development of gridded surface meteorological data for ecological applications and modelling. *Int J Climatol* 33: 121–131
- AghaKouchak A, Cheng L, Mazdiyasni O, Farahmand A (2014) Global warming and changes in risk of concurrent climate extremes: insights from the 2014 California drought. *Geophys Res Lett* 41: 8847–8852. doi:[10.1002/2014GL062308](https://doi.org/10.1002/2014GL062308)
- Alexander LV, Zhang X, Peterson TC et al (2006) Global observed changes in daily climate extremes of temperature and precipitation. *J Geophys Res* 111, D05109. doi:[10.1029/2005JD006290](https://doi.org/10.1029/2005JD006290)
- Almazroui M, Islam MN, Dambul R, Jones PD (2014) Trends of temperature extremes in Saudi Arabia. *Int J Climatol* 34:808–826. doi:[10.1002/joc.3722](https://doi.org/10.1002/joc.3722)
- Assessment report of China's ground temperature $0.5^\circ \times 0.5^\circ$ gridded dataset (V2.0) (2012) National Meteorological Information Center, Beijing
- Beniston M (2003) Climatic change in mountain regions: a review of possible impacts. *Climate Change* 59:5–31
- Beniston M, Rebetez M (1996) Regional behavior of minimum temperatures in Switzerland for the period 1979–1993. *Theor Appl Climatol* 53:231–243
- Brohan P, Kennedy JJ, Harris I, Tett SFB, Jones PD (2006) Uncertainty estimates in regional and global observed temperature change: a new data set from 1850. *J Geophys Res Atmos* 111, D12106. doi:[10.1029/2005JD006548](https://doi.org/10.1029/2005JD006548)
- Donat MG, Alexander LV (2012) The shifting probability distribution of global daytime and night-time temperatures. *Geophys Res Lett* 39, L14707. doi:[10.1029/2012GL052459](https://doi.org/10.1029/2012GL052459)
- Durre I, Wallace JM, Lettenmaier DP (2000) Dependence of extreme daily maximum temperature on antecedent soil moisture in the contiguous United States during summer. *J Clim* 13:2641–2651
- Easterling DR, Meehl GA, Parmesan C, Changnon SA, Karl TR, Mearns LO (2000) Climate extremes: observations, modeling, and impacts. *Science* 289:2068–2074
- Fan Z, Bräuning A, Thomas A, Li J, Cao K (2011) Spatial and temporal temperature trends on the Yunnan Plateau (Southwest China) during 1961–2004. *Int J Climatol* 31:2078–2090
- Frank T (2005) Climate change impacts on building heating and cooling energy demand in Switzerland. *Energy Build* 37:1175–1185
- Gao Y, Feng Q, Liu W, Lu A, Wang Y, Yang J, Cheng A, Wang Y, Su Y, Liu L, Ma Q (2014) Changes of daily climate extremes in Loess Plateau during 1960–2013. *Quat Int* 1–17. doi:[10.1016/j.quaint.2014.08.052](https://doi.org/10.1016/j.quaint.2014.08.052)
- Gu S, Yang X (2006) Variability of the northern circumpolar vortex and its association with climate anomaly in China. *Sci Meteorologica Sin* 26:135–142
- Guan Y, Zhang X, Zheng F, Wang B (2015) Trends and variability of daily temperature extremes during 1960–2012 in the Yangtze River Basin, China. *Glob Planet Chang* 124:79–94
- IPCC (2014) Climate change 2014: synthesis report. Contribution of Working Groups I, II and III to the Fifth Assessment Report of the Intergovernmental Panel on Climate Change. In: Core Writing Team, Pachauri RK and Meyer LA. (eds). IPCC, Geneva, 151 pp
- Kendall MG (1975) Rank correlation methods, 4th edn. Griffin, London, p 202
- Klein Tank AMG, Peterson TC, Quadir DA et al (2006) Changes in daily temperature and precipitation extremes in central and south Asia. *J Geophys Res* 111, D16105. doi:[10.1029/2005JD006316](https://doi.org/10.1029/2005JD006316)
- Li Z, He Y, Wang P, Theakstone WH, An W, Wang X, Lu A, Zhang W, Cao W (2012) Changes of daily climate extremes in southwestern China during 1961–2008. *Glob Planet Chang* 80–81:255–272
- Liang K, Bai P, Li J, Liu C (2014) Variability of temperature extremes in the Yellow River basin during 1961–2011. *Quat Int* 336:52–64
- Luterbacher J, Dietrich D, Xoplaki E, Grosjean M, Wanner H (2004) European seasonal and annual temperature variability, trends, and extremes since 1500. *Science* 303:1499–1503
- Mann HB (1945) Non-parametric tests against trend. *Econometrica* 13: 245–259
- Miranda PMA, Tome AR (2009) Spatial structure of the evolution of surface temperature (1951–2004). *Clim Chang* 93:269–284. doi:[10.1007/s10584-008-9540-8](https://doi.org/10.1007/s10584-008-9540-8)
- Otto FEL, Massey N, van Oldenborgh GJ, Jones RG, Allen MR (2012) Reconciling two approaches to attribution of the 2010 Russian heat wave. *Geophys Res Lett* 39, L04702. doi:[10.1029/2011GL050422](https://doi.org/10.1029/2011GL050422)
- Piao S, Ciais P, Huang Y, Shen Z, Peng S, Li J, Zhou L, Liu H, Ma Y, Ding Y (2010) The impacts of climate change on water resources and agriculture in China. *Nature* 467:43–51
- Ren GY, Ding YH, Zhao ZC, Zheng JY, Wu TW, Tang GL, Xu Y (2012) Recent progress in studies of climate change in China. *Adv Atmos Sci* 29:958–977
- Skaggs KE, Irmak S (2012) Long-term trends in air temperature distribution and extremes, growing degree-days, and spring and fall frosts for climate impact assessments on agricultural practices in Nebraska. *J Appl Meteorol Climatol* 51:2060–2073. doi:[10.1175/JAMC-D-11-0146.1](https://doi.org/10.1175/JAMC-D-11-0146.1)
- Stott P, Sone DA, Allen MR (2004) Human contribution to the European heatwave of 2003. *Nature* 432:610–613
- Sun Y, Zhang X, Zwiers FW, Song L, Wan H, Hu T, Yin H, Ren G (2014) Rapid increase in the risk of extreme summer heat in Eastern China. *Nat Clim Chang* 4:1082–1085. doi:[10.1038/NCLIMATE2410](https://doi.org/10.1038/NCLIMATE2410)
- Sun Q, Miao C, Duan Q, Wang Y (2015) Temperature and precipitation changes over the Loess Plateau between 1961 and 2011, based on high-density gauge observations. *Glob Planet Chang* 132:1–10. doi:[10.1016/j.gloplacha.2015.05.011](https://doi.org/10.1016/j.gloplacha.2015.05.011)
- Tao H, Fraedrich K, Menz C, Zhai J (2014) Trends in extreme temperature indices in the Poyang Lake Basin, China. *Stoch Env Res Risk A* 28:1543–1553. doi:[10.1007/s00477-014-0863-x](https://doi.org/10.1007/s00477-014-0863-x)
- Tian L, Yao T, Li Z, MacClune K, Wu G, Xu B, Li Y, Lu A, Shen Y (2006) Recent rapid warming trend revealed from the isotopic record in Muztagata ice core, eastern Pamirs. *J Geophys Res* 111: D13103. doi:[10.1029/2005JD006249](https://doi.org/10.1029/2005JD006249)

- Vallis GK, Zurita-Gotor P, Cairns C, Kidston J (2015) Response of the large-scale structure of the atmosphere to global warming. *Q J R Meteorol Soc* 141:1479–1501
- Vincent LA, Mekis E (2006) Changes in daily and extreme temperature and precipitation indices for Canada over the twentieth century. *Atmosphere-Ocean* 44:177–193. doi:[10.1029/2005JD006316](https://doi.org/10.1029/2005JD006316)
- Viola F, Liuzzo L, Noto LV, Conti FL, Loggia GL (2014) Spatial distribution of temperature trends in Sicily. *Int J Climatol* 34:1–17. doi:[10.1002/joc.3657](https://doi.org/10.1002/joc.3657)
- Wang A, Fu J (2013) Changes in daily climate extremes of observed temperature and precipitation in China. *Atmos Oceanic Sci Lett* 6: 312–319. doi:[10.3878/j.issn.1674-2834.12.0106](https://doi.org/10.3878/j.issn.1674-2834.12.0106)
- Wang Q, Zhang M, Wang S, Ma Q, Sun M (2014) Changes in temperature extremes in the Yangtze River Basin, 1962–2011. *J Geogr Sci* 24:59–75. doi:[10.1007/s11442-014-1073-7](https://doi.org/10.1007/s11442-014-1073-7)
- Wigley TML (1985) Climatology: impact of extreme events. *Nature* 316: 106–107
- Wu X, Wang Z, Zhou X, Lai C, Lin W, Chen X (2015) Observed changes in precipitation extremes across 11 basins in China during 1961–2013. *Int J Climatol*. doi:[10.1002/joc.4524](https://doi.org/10.1002/joc.4524)
- Xu X, Lin H, Hou L, Yao X (2002) An assessment for sustainable developing capability of integrated agricultural regionalization in China. *Chin Geogr Sci* 12:1–8
- Yang H, Yang D, Hu Q, Lv H (2014) Spatial variability of the trends in climatic variables across China during 1961–2010. *Theor Appl Climatol* 120:773–783. doi:[10.1007/s00704-014-1208-x](https://doi.org/10.1007/s00704-014-1208-x)
- You Q, Kang S, Pepin N, Yan Y (2008) Relationship between trends in temperature extremes and elevation in the eastern and central Tibetan Plateau, 1961–2005. *Geophys Res Lett* 35, L04704. doi:[10.1029/2007GL032669](https://doi.org/10.1029/2007GL032669)
- You Q, Kang S, Aguilar E, Pepin N, Flugel W, Yan Y, Xu Y, Zhang Y, Huang Z (2009) Changes in daily climate extremes in China and their connection to the large scale atmospheric circulation during 1961–2003. *Clim Dyn* 36:2399–2417. doi:[10.1007/s00382-009-0735-0](https://doi.org/10.1007/s00382-009-0735-0)
- Zhai P, Pan X (2003) Trends in temperature extremes during 1951–1999 in China. *Geophys Res Lett* 30(17):1913. doi:[10.1029/2003GL018004](https://doi.org/10.1029/2003GL018004)
- Zhang X, Vincent LA, Hogg WD, Niitsoo A (2000) Temperature and precipitation trends in Canada during the 20th century. *Atmosphere-Ocean* 38:395–429
- Zhang Q, Li J, Chen YD, Chen X (2011a) Observed changes of temperature extremes during 1960–2005 in China: natural or human-induced variations? *Theor Appl Climatol* 106:417–431. doi:[10.1007/s00704-011-0447-3](https://doi.org/10.1007/s00704-011-0447-3)
- Zhang X, Alexander L, Hegerl GC, Jones P, Tank AK, Peterson TC, Trewin B, Zwiers FW (2011b) Indices for monitoring changes in extremes based on daily temperature and precipitation data. *WIREs Clim Change* 2:851–870. doi:[10.1002/wcc.147](https://doi.org/10.1002/wcc.147)
- Zhang D, Xu W, Li J, Cai Z, An D (2013) Frost-free season lengthening and its potential cause in the Tibetan Plateau from 1960 to 2010. *Theor Appl Climatol* 115:441–450
- Zhang Z, Song X, Tao F, Zhang S, Shi W (2016) Climate trends and crop production in China at county scale, 1980 to 2008. *Theor Appl Climatol* 123:291–302. doi:[10.1007/s00704-014-1343-4](https://doi.org/10.1007/s00704-014-1343-4)
- Zhou Y, Ren G (2011) Change in extreme temperature event frequency over mainland China, 1961–2008. *Clim Res* 50:125–139. doi:[10.3354/cr01053](https://doi.org/10.3354/cr01053)